2019

The Total Solar Eclipse of 2017: Meteorological Observations from a Statewide Mesonet and Atmospheric Profiling Systems

Rezaul Mahmood

Megan Schargorodski

Eric Rappin

Melissa Griffin

Patrick Collins

See next page for additional authors

Authors

Rezaul Mahmood, Megan Schargorodski, Eric Rappin, Melissa Griffin, Patrick Collins, Kevin Knupp, Andrew Quilligan, Ryan Wade, Kevin Cary, and Stuart Foster

The Total Solar Eclipse of 2017: Meteorological Observations from a Statewide Mesonet and Atmospheric Profiling Systems

(Submitted to: *Bulletin of the American Meteorological Society*)

Rezaul Mahmood[*,1,2,3], Megan Schargorodski[2], Eric Rappin[2], Melissa Griffin[2,4,] Patrick Collins[2], Kevin Knupp[4], Andrew Quilligan[2], Ryan Wade[4], Kevin Cary[3], and Stuart Foster[2,3]

[2]Kentucky Climate Center and [3]Department of Geography and Geology
Western Kentucky University, Bowling Green, KY 42101

[4]Department of Atmospheric Science
University of Alabama in Huntsville, Huntsville, AL

*Corresponding author; E-mail: rmahmood2@unl.edu; Phone: 402- 472-6166

[1]Currently at the High Plains Regional Climate Center, School of Natural Resources, University of Nebraska-Lincoln, NE 68583

[4]Currently at the South Carolina State Climatology Office, Department of Natural Resources, Land, Water, and Conservation Division, Columbia, SC 29202

Early Online Release: This preliminary version has been accepted for publication in *Bulletin of the American Meteorological Society*, may be fully cited, and has been assigned DOI 10.1175/BAMS-D-19-0051.1. The final typeset copyedited article will replace the EOR at the above DOI when it is published.

Abstract: A total solar eclipse traversed the continental United States on August 21, 2017. It was the first such event in 99 years and provided a rare opportunity to observe the atmospheric response from a variety of instrumented observational platforms. This paper discusses the high-quality observations collected by the Kentucky Mesonet (www.kymesonet.org), a research-grade meteorological and climatological observation network consisting of 72 stations and measuring air temperature, precipitation, relative humidity, solar radiation, wind speed, and wind direction. The network *samples* the atmosphere, for most variables, every three seconds and then calculates and records observations every five minutes. During the total solar eclipse, these observations were complemented by observations collected from three atmospheric profiling systems positioned in the path of the eclipse and operated by the University of Alabama in Huntsville (UAH).

Observational data demonstrates that solar radiation at the surface dropped from > 800 to 0 W m^{-2}, the air temperature decreased by about 4.5 °C and, most interestingly, a land breeze/sea breeze-type wind developed. In addition, due to the high density of observations, the network recorded a detailed representation of the spatial variation of surface meteorology. The UAH profiling system captured collapse and reformation of the planetary boundary layer and related changes during the total solar eclipse.

Capsule: High density meteorological observations show notable response of the atmosphere and changes in measured variables during a historic solar eclipse.

Accepted for publication in *Bulletin of the American Meteorological Society.* DOI 10.1175/BAMS-D-19-0051.1.

On August 21, 2017 a total solar eclipse traversed the continental United States (Figure 1), the first to do so in 99 years, providing a rare opportunity to observe the atmospheric response from a variety of observational platforms. It reached the point of greatest eclipse over western Kentucky (near Hopkinsville, KY), allowing the Kentucky Mesonet to collect meteorological measurements with a high spatiotemporal density. This paper discusses the high-quality observations collected by the Kentucky Mesonet (www.kymesonet.org; S. Foster and R. Mahmood 2017, unpublished data; Mahmood et al. 2019) operated by Western Kentucky University and a mesoscale network of atmospheric profiling systems (20-30 km spacing), operated by University of Alabama in Huntsville (UAH) (K. Knupp 2017, unpublished data), along the path of totality near Hopkinsville, KY (Figures 2 and 3a-c) during this unique event. The Kentucky Mesonet is a research-grade meteorological and climate observation network (please see 'observed data' section and Mahmood et al. 2019 for details), consisting of 72 stations that collects air temperature, precipitation, relative humidity, solar radiation, wind speed and wind direction data. For most variables, the network samples the atmosphere every three seconds, calculates and records observations every five minutes and distributes them through the World Wide Web. Currently, 38 stations observe soil moisture and soil temperature data at five depths up to one meter. The UAH atmospheric profiling systems included wind profilers, thermodynamic profilers, lidar ceilometers, high-temporal resolution surface weather stations, and balloon soundings.

On the day of the eclipse, the Kentucky Mesonet recorded data every three seconds for incoming solar radiation, air temperature, wind direction, and wind speed. The Ohio and Tennessee River Valley experienced favorable weather (generally cloud-free) during the total

Accepted for publication in *Bulletin of the American Meteorological Society.* DOI 10.1175/BAMS-D-19-0051.1.

solar eclipse and as a result, ideal environmental conditions were in place for the Kentucky Mesonet to collect a wealth of data.

The network of three UAH atmospheric profiling systems collected thermodynamic and wind profiles every minute, as well as surface weather station data every five seconds for incoming solar radiation, air temperature, humidity, pressure, wind direction, and wind speed. Additionally, balloon soundings were launched every 1.5 hours from sunrise to sunset, and a mobile mesonet vehicle drove transects across varying land-cover types while recording observations every five seconds, like the stationary surface stations.

The objective of this paper is to analyze and report on responses of (i) the surface meteorological variables, and (ii) the planetary boundary layer (PBL) to the loss of solar forcing, due to a total solar eclipse. The study also addresses causation of the observed responses. The analyses include the spatiotemporal evolution of near-surface meteorological conditions, and the potential causes of the changes in these quantities. Weather Research and Forecasting (WRF; Skamarock et al. 2008) model simulations (E. Rappin 2018, unpublished data) with and without the solar eclipse, were conducted to compliment the observational analysis.

This research is extensive and complimentary to the studies conducted by Lee et al. (2018) and Turner et al. (2018). Lee et al. (2018) analyzed continental-scale meteorological data from the Climate Reference Network while Turner et al. (2018) assessed data from three closely located sites in north central Oklahoma that were far from the path of the totality. Our study is focused on the meso- and regional-scale response of the atmosphere observed by a statewide meteorological network and atmospheric profiling systems, augmented by atmospheric modeling.

Accepted for publication in *Bulletin of the American Meteorological Society.* DOI 10.1175/BAMS-D-19-0051.1.

Past studies have focused on meteorological response to a total solar eclipse. For example, Hanna (2000) analyzed data from a total solar eclipse that passed though the southwestern tip of the United Kingdom (U.K.) on August 11, 1999, primarily using air temperature, solar radiation, wind speed, and cloud cover observations from 81 amateur and official stations. Surface meteorology and air quality were also observed for the same total eclipse by two meteorological and four air quality observation sites in southern Germany (Ahrens et al. 2001). As in the U.K., observation conditions were not optimal due to cloud cover. Founda et al. (2007) analyzed data for the total solar eclipse of March 29, 2006 over Greece and applied the WRF model for further understanding of the atmospheric response. Our research adapted Founda et al.'s (2007) approach.

In a series of papers, Gray and Harrison (2016), Hanna et al. (2016), Clark (2016), Clark (2016), and Barnard et al. (2016) investigated the impacts of a partially obscured (by cloud cover) total solar eclipse on the surface meteorology in the British Isles that occurred on March 20, 2015 over the North Atlantic Ocean in a region between the British Isles and Iceland. A number of these studies used data from a road-weather network and citizen scientists along with standard meteorological observation sites maintained by the Met Office. All of these studies recorded lowering of solar radiation and air temperature after the beginning of the eclipse. Solar radiation reached zero W m^{-2} while air temperatures dropped several degrees Celsius during totality. After the end of the totality phase and through the partial eclipse phase, solar radiation and air temperature increased, as expected. In addition, lowering of wind speed, changes in wind direction, and increase of relative humidity were also observed during the evolution of eclipse.

Founda et al. (2007) noted that each solar eclipse study is unique because of differences in background synoptic conditions, geographic location, season, and time of day. Indeed, the

Accepted for publication in *Bulletin of the American Meteorological Society.* DOI 10.1175/BAMS-D-19-0051.1.

2017 solar eclipse provided an opportunity to investigate a total solar eclipse under a unique setting. This included clear sky conditions (as opposed to cloudy conditions) with the sun near its zenith, a distinctive geographic region characterized by a complex topographic backdrop, and an infrastructure for collecting surface meteorological observations that fulfills the expectation of homogeneity of observations (i. e, instrumentation, sampling, maintenance, and exposure).

The study presents results from the analysis of data collected during the total solar eclipse of August 21, 2017 as it traversed Kentucky where totality reached its maximum time-length. The remainder of the paper provides a description of the collected data, geographic setting, synoptic background, results from WRF simulations, and final remarks.

Observed Data

Kentucky Mesonet

As noted above, the Kentucky Mesonet collects data across the state. The network ensures that observing stations are located in sites representative of the geography of the area such as land cover and terrain, and meet scientific criteria for station and instrument exposure. The latter two items require that stations are located in open areas, away from natural obstructions including trees or human-made structures (e.g., buildings, asphalts, roads etc.) to minimize potential bias in observations. Stations are well-maintained with three seasonal site passes where mesonet field technicians conduct prescribed maintenance procedures from cleaning of sensors to checking calibration. In addition, the network produces twice-daily reports for maintenance tickets. Incoming five-minute data pass through an automated quality assurance (QA) process. Questionable data get flagged and site maintenance tickets are issued, as

Accepted for publication in *Bulletin of the American Meteorological Society.* DOI 10.1175/BAMS-D-19-0051.1.

warranted. Technicians make site visits based on these tickets, with the nature of the issue dictating the required response time.

To reduce measurement bias, the Kentucky Mesonet uses high-quality and redundant sensors. For example, to measure air temperature, the network uses three air temperature sensors located within a aspirated radiation shield. Moreover, if air temperature measurements differ by a value equal to or larger than 0.3 °C between two sensors then data are flagged. Given the impact of a solar eclipse on air temperature, this care in data collection and operational approach ensures high-quality data during the solar eclipse.

For most observed variables, including air temperature, the mesonet stations take sensor measurements (i.e., samples) every three seconds over a five-minute period and then calculate and report five-minute observations as an average of the three-second samples. The data subsequently are transmitted from the station to the computer servers via cell communication for further processing (e.g., QA) and archiving. For this historic solar eclipse event, it was decided that the Kentucky Mesonet would record and report data every three seconds for air temperature, incoming solar radiation, wind speed, and wind direction for all stations, with the other quantities coming in at the standard five-minute interval. Thus, the network not only brought near real-time data from stations within the path of totality but also from stations that were not within the path, permitting a detailed investigation of the spatial and temporal variation in measured quantities.

To ensure the accuracy of observations for the solar eclipse in 2017, the Kentucky Mesonet took a number of additional steps. First, the solar radiation sensors were replaced with the new sensors of the same model. Deployment of the new sensors was completed during summer site maintenance pass to make sure that all sensors in the field were less than one year old. Second, seasonal site maintenance passes were scheduled to ensure completion immediately

Accepted for publication in *Bulletin of the American Meteorological Society.* DOI 10.1175/BAMS-D-19-0051.1.

prior to the eclipse. Third, to test the ability of the Mesonet to successfully collect and communicate data to the Mesonet computer servers and general public, and archive three-second data during this historic event, the network completed 'trial runs' for the customized data collection. Mesonet staff contacted the cell provider to ensure that the network received a priority status in case of a congested cell network on the day of the event due to the increased cell communication (due to eclipse viewers) in the area. All of these suggest a significant effort by the network's instrumentation technology, information technology, and staff.

Atmospheric Profiling Systems

The University of Alabama in Huntsville fielded three mobile atmospheric profiling systems and a mobile Doppler radar, among others (Figure 3b-c). The profiling systems and their components included the Mobile Integrated Profiling System (MIPS) (which includes a 915 MHz wind profiler, X-band profiling radar, microwave profiling radiometer, lidar ceilometer, and surface instrumentation); the Rapidly Deployable Atmospheric Profiling System (RaDAPS) (which includes a 915 MHz wind profiler, microwave profiling radiometer, lidar ceilometer, and surface instrumentation); and the Mobile Doppler Lidar and Sounding system (MoDLS) (which includes Doppler wind lidar, microwave profiling radiometer, and surface instrumentation).

Radiosondes were launched at 1.5 hour intervals from all three profiling systems around the time of the eclipse. The Mobile Alabama X-band (MAX) was deployed adjacent to the MIPS, but data from it are not included in this analysis. The MIPS, RaDAPS and MoDLS were deployed in a triangular array in Christian County, Kentucky with separation distances of 20-30 km, as illustrated in Figure 2. The goal was to deploy these systems in different land use regimes in order to document mesoscale variability within the PBL. The profilers were located in the

Accepted for publication in *Bulletin of the American Meteorological Society.* DOI 10.1175/BAMS-D-19-0051.1.

following areas: MIPS within an agricultural region with a field of corn on one side and soybeans on the other; RaDAPS within a forested region along the eastern fringe of the Land Between the Lakes; and MoDLS within a region mixed with grass and scattered trees.

Synoptic Environment

In Kentucky, the synoptic setting was ideal for observing the total eclipse. The day of the solar eclipse was dry with clear skies which allowed the networks to observe changes of solar radiation with the evolution of the eclipse. A qualitative assessment shows that the Bermuda high had settled into the southeastern United States. Regional surface atmospheric pressure was around 1022 mb. As a result, the skies were mostly clear with only widely scattered cumulus clouds, and the winds were weak along the path of totality across the state. Kentucky and its surrounding region generally observed much greater than 5 °C dew point depression, indicative of relatively dry atmosphere (Supplementary Figure 1). A stationary front was located over the upper Midwest and the northern Great Plains.

Observed surface meteorological response: regional and in and around the path of totality

Solar radiation at the surface

As an example, data are presented from the Kentucky Mesonet site at Warren County, which is located on a large farm owned by Western Kentucky University close to the Kentucky Mesonet's main operations center. Figure 4a shows both three-second data and the same data that was smoothed with a five-minute moving-window filter. Since three-second data are noisy, only the filtered data will be presented from here on. On a clear, stable day like August 21, 2017, the expected smooth rise of solar radiation was observed after sunrise and throughout the

Accepted for publication in *Bulletin of the American Meteorological Society.* DOI 10.1175/BAMS-D-19-0051.1.

morning (local time). Around ~1700 UTC (12:00 pm local time), as the partial solar eclipse arrived in this region, solar radiation started to decline from its peak of about 850 W m^{-2}. Just prior to 1830 UTC (1:30 pm local time), solar radiation observation was reduced to 0 W m^{-2} (unsmoothed three-second data) as totality settled in. As totality ended, the observed solar radiation also steadily increased until the partial eclipse ended around 2000 UTC (~3:00 pm local time) and subsequently solar radiation declined following the diurnal cycle.

The regional response of solar radiation can be seen from the Kentucky Mesonet (Figure 5a-c) data. These figures show that solar radiation was near 850 W m^{-2} at the beginning (1705 UTC) of the solar eclipse, decreasing to 0 W m^{-2} for the stations experiencing totality (1825 UTC), and then increasing back to close to 800 W m^{-2} by the end of the eclipse (1945 UTC).

The response of solar radiation and its reduction observed by the Kentucky Mesonet is consistent with the findings from Lee et al. (2018) and Turner et al. (2019). Note that the observations from the latter study were not exposed to the full total eclipse and did not focus on the surface meteorology, possibly because data were collected from only three locations. On the other hand, as noted previously, Lee et al. (2018) focused on the continental-scale. Our study nicely shows changes in solar radiation at the meso-scale under total eclipse and fills a void of observations and findings between micro and continental-scales. Another unique aspect of this study is that this is the first time a meso-scale observation platform assessed solar radiation during a total eclipse in the United States.

Meteorological observations and analyses were completed for a limited number of in-situ sites in the southwest of Germany during a total solar eclipse on August 11, 1999 (Ahrens et al. 2001). This total eclipse occurred in the late morning (~11:30 am local time) and solar radiation declined to zero W m^{-2}, like in Kentucky. Observations suggest that clouds were present leading

Accepted for publication in *Bulletin of the American Meteorological Society.* DOI 10.1175/BAMS-D-19-0051.1.

up to the total eclipse and during the post-eclipse recovery of solar radiation in Germany. In other words, solar radiation decline was not 'smooth' as was observed in Kentucky where clear skies prevailed. Hence, observations in Kentucky provided a better opportunity to verify our conceptual understanding of solar radiation changes during a total eclipse.

During the total eclipse of March 20, 2015 over the North Atlantic/North Sea region, surface meteorological observations and data analyses were completed for the British Isles and Iceland (Barnard et al. 2016; Gray and Harrison 2016; Hanna et al. 2016; and Pasachoff et al. 2016). However, these studies either did not include analyses of solar radiation or provided limited assessments. Nevertheless, surface data collected during a radiosonde launch from Reading, U.K., reported approximately 10 W m^{-2} of solar radiation, representing an approximate 30 W m^{-2} reduction during the near-peak eclipse (note that the U.K. did not experience a total eclipse) (Burt 2016). This small reduction was partly linked to the local mid-morning cloud cover near-total eclipse. Note that a study by Harrsion et al. (2016) measured solar radiation from three locations in U.K. and Iceland during this eclipse using weather balloons. As anticipated, data from this study reports reduction of solar radiation. However, again, this study did not observe detailed surface solar radiation.

Surface temperature and relative humidity

The air temperature cycle of this day was an example of the diurnal evolution during a total solar cycle as seen in Figure 4a for the Warren County site. On this day, a few minutes after the observed solar radiation maximum, the air temperature peaked at 32.5 °C in the morning (local time). After the commencement of the partial solar eclipse, the air temperature

Accepted for publication in *Bulletin of the American Meteorological Society.* DOI 10.1175/BAMS-D-19-0051.1.

declined following the reduction of incoming solar radiation. During totality the air temperature declined to 28.0 °C, a 4.5 °C reduction, as the eclipse proceeded from partial to total.

Regional changes in air temperature can also be seen from the Kentucky Mesonet (Figure 5a-c) data. These figures show that air temperatures were in the lower 30s °C during the beginning (1705 UTC) of the solar eclipse, decreased to the upper 20s °C near totality (1825 UTC), and then increased back to the lower 30s °C (1945 UTC). In other words, several locations recorded an average 1 °C air temperature decrease every 15 minutes during the eclipse's path of totality.

In Germany air temperature declined greater than 5 °C during the eclipse maximum of total solar eclipse of 1999 (Ahrens et al. 2001). During the total solar eclipse of 2015 over the North Atlantic, air temperature reductions over the U.K. and Iceland were mostly less than 2 °C (Hanna et al., 2016). It is possible that the morning timing for the eclipse and cloud cover dampened the magnitude of air temperature decline. Again, analyses presented from our research provide additional perspective of air temperature decline during a total eclipse in the afternoon under clear sky condition.

Due to stable conditions from the Bermuda High and absence of widespread large-scale flow of moisture from the Gulf of Mexico changes in relative humidity were largely linked to changes in air temperature. Data from Warren County show that air temperature increased and relative humidity decreased as the morning progressed. However, with the commencement of the eclipse and the absence of solar forcing, air temperature declined and relative humidity steadily increased. The latter decreased from its peak of about 75% in the early morning to near 40% prior to the beginning of the solar eclipse (Figure 4a). On the other hand, during totality relative humidity rapidly increased to about 60%. After the end of the eclipse relative humidity

Accepted for publication in *Bulletin of the American Meteorological Society.* DOI 10.1175/BAMS-D-19-0051.1.

again decreased to about 42%. Subsequently, relative humidity slowly increased, following its diurnal cycle. Regionally, relative humidity also showed a spatiotemporal pattern through the evolution of the solar eclipse reflecting proximity to the path of the totality (Figure 5a-c).

Further assessment suggests that compared to the relative humidity in Kentucky, changes in relative humidity during a total eclipse in 1999 in Germany was notably muted. There was a near 7% rise in relative humidity in Germany compared to about 25% in Kentucky (Ahrens et al. 2001). In the U.K., change in relative humidity during 2015 near total eclipse was also minimal and comparable to the magnitude observed in Germany (e.g., Gray and Harrison 2016). It is suggested that the timing of the mid-morning eclipse did not allow a larger reduction in relative humidity (following its typical diurnal cycle) and then subsequent increase during the eclipse.

Surface wind

Due to high pressure over the region, the weak wind primarily reflected thermal forcing from daytime solar heating. With the loss of daytime heating during the eclipse, the thermal circulation began to collapse as the boundary layer began to stabilize. At Warren County, the wind speed reached its peak of 2.75 m s^{-1} about an hour before totality and then fell to 0.5 m s^{-1} (Figure 4b). The latter was about 40 minutes after totality and 100 minutes after reaching a maximum. It is suggested that the decline and subsequent absence of solar forcing during the progression of and during the total solar eclipse, respectively, resulted in the decline of wind speed and the near calm conditions. In addition, at the Warren County site, wind direction veered from southwesterly to northwesterly during totality.

To further assess these findings regarding solar radiation, air temperature, relative humidity, and wind speed and direction, data from stations located in Todd, Christian, and Trigg

Accepted for publication in *Bulletin of the American Meteorological Society.* DOI 10.1175/BAMS-D-19-0051.1.

County were analyzed (Figure 6a-f). These three stations (Christian and Trigg are immediate western counties relative to Todd) are in close proximity to one another (Figure 2), zonally oriented, and all within the path of totality. Solar radiation was reduced from over 800 to 0 W m^{-2} from prior to the eclipse to totality at each station. Following this pattern, air temperatures also declined, at some sites more than 4 °C. The peak decline at each location lagged by up to 15 minutes compared to the timing of totality as buoyant turbulence takes time to dissipate as the boundary layer stabilizes. As noted above, there was little large-scale moisture advection (e.g., from the Gulf of Mexico) and hence, relative humidity followed the air temperature evolution and declined as day progressed in advance of the solar eclipse. All three stations show a rapid rise from about 45% to about 75% during totality. Following the eclipse, relative humidity quickly lowered to near 50% or lower. As solar radiation returned, air temperature also increased and relative humidity declined to near pre-eclipse levels.

Wind speed steadily declined once the eclipse commenced, reaching a minimum during totality. At Todd County, wind speed declined from its maximum of about 2.5 to 0 m s^{-1} during the total eclipse. As noted previously, change in wind speed was likely to be linked to cessation of solar heating of the land surface. Surface wind backed at all three locations and as totality ended the wind direction veered (clockwise) back to near its original direction. Regionally, the response of surface wind was similar to the above observations, i.e., generally backing during the totality and veering towards the pre-eclipse direction after the end of the totality (Figure 5a-c).

A comparison of wind observations from Germany and the U.K. suggests that the response of the wind in Kentucky during the total eclipse was consistent with previous observations under total and partial solar eclipses in the other parts of the world. It was found that wind speed declined about 2.75 m s^{-1} in Germany (Ahrens et al. 2001) and 1 m s^{-1} in the

Accepted for publication in *Bulletin of the American Meteorological Society.* DOI 10.1175/BAMS-D-19-0051.1.

U.K. (Gray and Harrison 2016), comparable to observations by the Kentucky Mesonet. Backing of the wind was also reported in the U.K. (Gray and Harrison 2016), which is consistent with our findings in the Kentucky observations.

Observed planetary boundary layer response

The response of the planetary boundary layer (PBL) to the reduction in solar radiation was quite prominent. Figure 7a-b and Figure 8a-b present time-versus-height sections of lidar backscatter (Figure 7a), vertical motion (Figure 7b), 915 MHz radar backscatter, expressed as a signal to noise ratio (SNR, Figure 8a), and 915 MHz radar spectrum width (SW, Figure 8b) which is a proxy for sub-grid scale turbulence. Each figure includes the time of totality (vertical solid line) and times of 50% totality before and after totality. The characteristic growth of the PBL occurred under mostly clear skies, and is clearly evident in the lidar vertical motion and 915 SNR and SW. Initial growth is indicated near 1400 UTC, and a maximum PBL height of ~1.6 km above ground level (AGL) is indicated near 1750 UTC. The Doppler Wind Lidar (DWL) vertical velocity (w) field also indicates a prominent thermal extending up to the same height of 1.6 km AGL at 1750 UTC.

The most prominent eclipse signal is the rapid reduction in turbulent motions within the PBL, shown directly in the lidar 1 Hz w (Figure 7b) and 915 SW. Both measurements reveal a PBL collapse from the top down, with significant DWL vertical motions and 915 turbulence both decreasing to low values prior to totality. A quick growth of the PBL resumed near 1940, about 25 minute after the 50% totality mark. This growth is much faster than the natural PBL growth between 1500 and 1800 UTC according to the 915 SNR and SW fields (Figure 8a-b). The top of the PBL following the eclipse (1.4 km) was about 0.2 km lower prior to the eclipse. A

Accepted for publication in *Bulletin of the American Meteorological Society.* DOI 10.1175/BAMS-D-19-0051.1.

pronounced time lag of about one hour in boundary layer collapse and restoration is noted in both the DWL and 915 SNR and SW measurements, consistent with more limited measurements during previous solar eclipse events (Turner et al. 2018).

Further inspection of the DWL *w* patterns reveals the presence of regular wave motions, which appear to be most significant near the capping inversion around the time of totality. Such wave motions would be expected to be most prominent near the capping inversion where the static stability is greatest. More irregular and lower amplitude oscillations in *w* appear at lower levels and dampen with time.

The thermodynamic response is illustrated in the radiometer-derived air temperature (Figure 9a-b) as cooling was confined to levels below about 100 m AGL. This signal is also time-lagged by about 15-20 minutes with respect to totality. Balloon soundings from the MIPS and RaDAPS sites (Figure 9a-b) confirm that cooling of 1.5-3.0 °C was confined to levels below ~100 m, compared to nocturnal radiational cooling of 6.0-8.0 °C and a depth of ~200 m for the soundings launched earlier in the morning just after sunrise. A corresponding increase in water vapor (dew point temperature---T_d) accompanied this cooling, and is consistent with the reduction in turbulent water vapor flux and evapotranspiration confined to a shallow, stable surface layer (e.g., Wingo and Knupp 2015). This increase in low-level water vapor was a permanent feature (Figure 9b), likely a consequence of water vapor advection within the PBL. We suggest that there were meso-scale variations in water vapor. For example, the surface dewpoint was higher at the RaDAPS site (near the 'Land between the Lakes' area, close to two large man-made lakes in Kentucky) than at the MIPS or MoDLS sites. In other words, advection from local moisture source impacted nearby measurements.

Accepted for publication in *Bulletin of the American Meteorological Society.* DOI 10.1175/BAMS-D-19-0051.1.

382 The Microwave Profiling Radiometer (MPR) air temperature field reveals an unexpected
383 warm column (air temperature perturbation of about 1.5 °C) within the 500-600 m AGL layer
384 above the low-level cool pool. This warming is consistent with subsidence measured directly by
385 the DWL around the time of totality (Figure 7b), yet warming would not be expected within
386 descending air if the residual layer had a constant potential temperature with height. Even the
387 water vapor field above about 300 m above surface suggests a local minimum around this time,
388 consistent with subsidence. Post-eclipse soundings confirmed the surface and PBL recovery
389 with the 2100 UTC sounding exhibiting a well-mixed, nearly dry adiabatic PBL down to the
390 surface, and the 2230 UTC sounding indicating a superadiabatic surface layer, although not as
391 deep as the 1700 UTC pre-eclipse sounding (Supplementary Figure 2a-d).
392
393 **The Weather Research and Forecasting Model Applications**
394 To further explore the impacts of the 2017 total solar eclipse and for comparison with
395 observations, the Weather Research and Forecasting (WRF) model (Skamarock et al. 2008)
396 version 3.7.1 was utilized. This version was specifically adapted for the study of the evolution of
397 the atmosphere during solar eclipses (Montornes et al. 2016). A 30-hour simulation from 0000
398 UTC, August 21, 2017 to 0600 UTC, Aug 22, 2017 was conducted with and without the
399 presence of the eclipse (i.e. without and with solar forcing, respectively). The total eclipse
400 occurred at roughly 1830 UTC on Aug 21, 2017 and hence, sufficient time was given for
401 dynamic adjustment. A single domain with 2 km grid spacing in the horizontal was adopted. In
402 addition, 38 levels in the vertical with 15 levels in the lowest 2 km of the atmosphere were
403 prescribed. Thompson microphysics (Thompson et al. 2008), RRTMG longwave and shortwave
404 radiation (Iacono et al. 2008), the Mellor-Yamada-Janjic (MYJ) boundary layer scheme (Janjic

Accepted for publication in *Bulletin of the American Meteorological Society.* DOI 10.1175/BAMS-D-19-0051.1.

1994), and the Noah land surface model (Chen and Dudhia 2001; Tewari et al. 2004) were selected for simulations. No convective parametrization was used.

The WRF model simulations were assessed against observed (Figure 10) data from the Kentucky Mesonet. This comparison showed that the model satisfactorily captured changes in solar radiation and air temperature as the eclipse slowly reached totality and eventually concluded. The simulations are in phase with the observations. In particular, the best agreement was observed from the beginning to the end of solar eclipse (Figure 10). During totality, simulated solar radiation, like observations, reached 0 W m^{-2} and air temperature dropped to 28.7 °C. These agreements provided further confidence in our model-based assessment.

Further assessment of the regional response to the total solar eclipse was conducted based on the WRF simulations. In this case, we focused on the period starting and ending at 1740 and 1940 UTC, respectively, capturing the duration of the eclipse, including totality. Modeled data for solar radiation (not shown), air temperature (supplementary Figure 3a-i), sensible heat (Figure 11a-i), and latent heat fluxes (Figure 12a-i) were analyzed for 'no solar eclipse' minus 'with total eclipse' scenarios. Simulations suggest that as the solar eclipse was commencing to the west of Kentucky over Missouri and Arkansas, we find large differences up to ~600 W m^{-2} solar radiation. During totality, this difference was up to ~1000 W m^{-2} over Kentucky. As the eclipse was ending across the region, the differences decreased to less than 100 to 200 Wm^{-2}. Air temperature, sensible, and latent heat fluxes follow the same pattern. For example, air temperature differences were up 2 °C in Missouri and Arkansas at 1740 UTC (Supplementary Figure 3a), up to 6 °C in western Kentucky and surrounding regions at 1825 UTC (Supplementary Figure 3d), while they diminished to less than 2 °C at 1940 UTC when solar eclipse was ending (Supplementary Figure 3i).

Accepted for publication in *Bulletin of the American Meteorological Society.* DOI 10.1175/BAMS-D-19-0051.1.

Differences in sensible heat fluxes were less than 200 W m^{-2} in Arkansas and most of Missouri and 50-100 W m^{-2} over most of Kentucky (Figure 11a). Close to totality, these differences were of similar magnitude but more widespread over these two states (Arkansas and Missouri). In Kentucky, close to totality differences were closer 150 W m^{-2} (Figure 11d) and largely diminished by 1940 UTC (Figure 11i). Differences in latent heat fluxes over most of Kentucky were between 150-200 W m^{-2} (Figure 12a) while close to totality they were largely about 500 W m^{-2}. Again these differences were reduced by 1940 UTC (Figure 12i).

A summary of these modeled results from four locations coinciding with Kentucky Mesonet sites is provided in Table 1. Recall that Todd, Christian, and Warren Counties are located within the path of the totality (Supplementary Figure 2). It was found that latent and sensible heat fluxes were higher in the without-solar-eclipse simulation. For example, at the beginning of the eclipse over Todd County, latent heat fluxes were 377 and 404 W m^{-2} with and without eclipse, respectively (Table 1). The sensible heat flux, meanwhile, was 137 and 157 W m^{-2} for simulations with and without solar eclipse, respectively. As evident, energy balance was continuously dominated by latent heat flux at all locations during the eclipse evolution (Table 1). Moreover, the most spectacular reduction of fluxes occurred geographically near the path of totality. For example, again, at Todd County, latent heat fluxes were reduced from 377 to 3 W m^{-2} and sensible heat flux from 137 to -11 W m^{-2} at the beginning of the solar eclipse and during the total solar eclipse, respectively. These findings are generally representative for the other three locations. Toward the end of the solar eclipse, fluxes were restored and differences between fluxes with and without solar eclipse diminished (Table 1).

Like the observed data, modeled air temperatures declined during totality. At the beginning, differences were almost non-existent. However, during totality the air temperature

Accepted for publication in *Bulletin of the American Meteorological Society.* DOI 10.1175/BAMS-D-19-0051.1.

declined 2.5 to 4 °C, which largely resembles Kentucky Mesonet observations. As anticipated, modeled planetary boundary layer heights also show notable lowering during totality. At Todd County site the planetary boundary layer was reduced to 43 m as boundary layer convective mixing ceased, while it was 1335 m at the beginning of the eclipse. The WRF simulations found that it would be 1899 m in the absence of the eclipse. These findings are consistent with our observations discussed previously and shown in Figure 7a-b.

Wind speeds showed a reduction of up to a 1.3 m s^{-1} from the beginning of the solar eclipse (3.0 m s^{-1}) to during totality (1.7 m s^{-1}) over Christian County. Like observations, modeled data suggest backing of wind during or near totality and then veering near the end of the eclipse. Relative humidity in the modeled data increased from the beginning of the solar eclipse to the total solar eclipse and subsequently declined at the end of the eclipse, as found in the observed data. However, compared to observations, the magnitude of these changes in wind direction and relative humidity was muted under simulations.

Finally, soundings from the four sites listed in Table 1 are shown in Supplementary Figure 4a-h for both simulations (with eclipse in magenta, without in black) at 1825 UTC (totality) and 1905 UTC (post-totality). Prior to the onset of the eclipse, convective mixing maintained a well- mixed boundary layer. At and after totality, moisture values above the surface but below the capping inversion decrease due to the loss of buoyancy at all sites as reflected in the dew point temperature. After the eclipse, prior to full boundary layer recovery, the dew point depression grew in magnitude. Given the synoptic setting, it is unsurprising that the boundary layer did not saturate except in the Todd county location near the base of the capping inversion. In terms of air temperature, the biggest declines are at the surface with larger boundary layer changes beneath the inversion after totality.

Accepted for publication in *Bulletin of the American Meteorological Society.* DOI 10.1175/BAMS-D-19-0051.1.

Summary

This research presented key findings highlighting the atmospheric response during a total solar eclipse that traversed the continental United States on August 21, 2017. Atmospheric observations were collected by the Kentucky Mesonet at Western Kentucky University and by three atmospheric profiling systems operated by the University of Alabama in Huntsville and positioned in southwestern Kentucky within the overall footprint of the Mesonet. The WRF model was also applied to provide simulations of the atmospheric response to the eclipse to supplement the observational data.

The Kentucky Mesonet data show that solar radiation at the surface decreased from > 800 Wm^{-2} to 0 W m^{-2}, the air temperature decreased by about 4.5 °C, and surface wind speed decreased more than 2 m s^{-1} (to ~0.5 m s^{-1}) during the total solar eclipse. Data also reported backing of wind during the total eclipse (southwesterly/southerly to southeasterly) and subsequent veering to pre-totality direction after the end of the totality. There was a steady decline of relative humidity as the day progressed, followed by a sharp increase to nearly 40% (from ~40 to ~80%) during the totality and a subsequent decline after the end of the totality.

The UAH profiling system captured collapse and reformation of the PBL and related changes during the total eclipse. Observations suggest a maximum PBL height of ~1.6 km near the 50% totality (1750 UTC) with a complete collapse during totality. A quick growth of the PBL resumed around 1940 UTC. A PBL recovery was observed by 2100 UTC and sounding data suggest that it was well-mixed with a nearly constant potential temperature.

The WRF model was applied with and without the solar eclipse to further understand atmospheric response. Assessment of the regional response suggested up to ~1000 W m^{-2} difference in solar radiation between with and without solar eclipse. Air temperature and both

Accepted for publication in *Bulletin of the American Meteorological Society.* DOI 10.1175/BAMS-D-19-0051.1.

sensible and latent heat fluxes followed the same pattern. At Todd County location, simulated latent heat fluxes decreased from 377 to 3 W m^{-2} and sensible heat flux from 137 to -11 W m^{-2} under no solar eclipse and total solar eclipse, respectively. During totality the simulated air temperature decreased from 2.5 - 4 °C, broadly consistent with Kentucky Mesonet observations. Modeled PBL heights also show, as expected, lowering or collapse during totality. For example, in Todd County, the PBL was reduced to 43 m as boundary layer convective mixing ceased, while it was 1335 m at the beginning of the eclipse. Simulated wind speeds also showed up to a 1.3 m s^{-1} reduction from the beginning of the solar eclipse (3.0 m s^{-1}) to the period of totality (1.7 m s^{-1}) over Christian County in Kentucky.

This research provided an unprecedented opportunity to document atmospheric response of a historic solar eclipse at the meso- and regional-scales by analyzing data from a statewide meteorological and climatological observation network and atmospheric profiling systems which were complemented by regional modeling. Observations and modeling work supported our conceptual understanding of potential atmospheric response due to the absence of solar radiation during the height of a summer season day. Finally, this research is complimentary to local- or continental-scale studies on the same topic and offered additional insight on the atmospheric response to total solar eclipse for these scales.

Acknowledgements: The authors would like to thank three anonymous reviewers and editor for their valuable comments which helped to improve this paper. Thanks also go to Joesph Matus for the total eclipse photo (Figure 1).

Accepted for publication in *Bulletin of the American Meteorological Society.* DOI 10.1175/BAMS-D-19-0051.1.

References:

Ahrens, D., G. M. Iziomon, L. Jaeger, A. Matzarakis, and H. Mayer, 2001: Impacts of the solar eclipse of 11 August 1999 on routinely recorded meteorological and air quality data in south-west Germany. *Meteorol. Z.,* **10,** 215–223.

Barnard L, Portas AM, Gray SL, Harrison RG. 2016 The National Eclipse Weather Experiment: an assessment of citizen scientist weather observations. *Phil. Trans. R. Soc. A,* **374**: 20150220. http://dx.doi.org/10.1098/rsta.2015.0220

Burt S., 2016: Meteorological responses in the atmospheric boundary layer over southern England to the deep partial eclipse of 20 March 2015. *Phil. Trans. R. Soc. A* **374**, 20150214.

Chen, F. and J. Dudhia, 2001: Coupling an advanced land surface–hydrology model with The Penn State–NCAR MM5 modeling system.Part I: Model implementation and sensitivity. *Mon. Wea. Rev.,* **129,** 569-585.

Clark, M.R., 2016: On the variability of near-surface screen temperature anomalies in the 20 March 2015 solar eclipse. *Phil. Trans. R. Soc. A* **374**, 20150213. http://dx.doi.org/10.1098/rsta.2015.0213

Clark, P. A., 2016: Numerical simulations of the impact of the 20 March 2015 eclipse on UK weather. *Phil. Trans. R. Soc. A*, **374**, 20150218. http://dx.doi.org/10.1098/rsta.2015.0218

Founda, D., D. Melas, S. Lykoudis, I. Lisaridis, E. Gerasopoulos, G. Kouvarakis, M. Petrakis, and C. Zerefos, 2007: The effect of the total solar eclipse of 29 March 2006 on meteorological variables in Greece. *Atmos. Chem. Phys.*, **7,** 5543–5553.

Gray, S. L., and R. G. Harrison, 2016: Eclipse-induced wind changes over the British Isles on the 20 March 2015. *Phil. Trans. R. Soc. A* **374**, 20150224.

Hanna, E., 2000: Meteorological effects of the solar eclipse of 11 August 1999. *Weather*, **55,** 430–446.

Hanna, E., J. Penman, T. Jónsson, G. R. Bigg, H. Björnsson, S. Sjúrðarson, M. A. Hansen, J. Cappelen, and R. G. Bryant, 2016: Meteorological effects of the solar eclipse of 20 March 2015: analysis of UK Met Office automatic weather station data and comparison with automatic weather station data from the Faroes and Iceland. *Phil. Trans. R. Soc. A*, **374**, 20150212. http://dx.doi.org/10.1098/rsta.2015.0212

Harrison, R. G., G. J. Marlton, P. D. Williams and K. A. Nicoll, 2016: Coordinated weather balloon solar radiation measurements during a solar eclipse. *Phil. Trans. R. Soc. A* **374**, 20150221. http://dx.doi.org/10.1098/rsta.2015.0221

Iacono, M. J., J. S. Delamere, E. J. Mlawer, M. W. Shephard, S. A. Clough, and W. D. Collins,

Accepted for publication in *Bulletin of the American Meteorological Society.* DOI 10.1175/BAMS-D-19-0051.1.

2008: Radiative forcing by long–lived greenhouse gases: Calculations with the AER radiative transfer models. *J. Geophys. Res.*, **113**, D13103.

Janjic, Z. I., 1994: The step-mountain Eta coordinate model: Further developments of the convection, viscous sublayer, and turbulence closure schemes. *Mon. Wea. Rev.*, **122**, 927–945.

Lee, T. R., M. Buban, M. A. Palecki, R. D. Leeper, H. J. Diamond, E. Dumas, T. P. Meyers, and C. B. Baker, 2018: Great American Eclipse data may fine-tune weather forecasts. *Eos*, **99,** https://doi.org/10.1029/2018EO103931.

Mahmood, R., M. Schargorodski, S. Foster, and A. Quilligan, 2019: A technical overview of the Kentucky Mesonet. *J. Amos. Oceanic Tech.* **36,** 1753-1771.

Montornès, A., B. Codina, J. W. Zack, and Y. Sola, 2016: Implementation of Bessel's method for solar eclipses prediction in the WRF-ARW model. *Atmos. Chem. Phys.*, **16,** 5949–5967.

Pasachoff, J. M., M. A. Peñaloza-Murillo, A. L. Carter, M. T. Roman, 2016: Terrestrial atmospheric responses on Svalbard to the 20 March 2015 Arctic total solar eclipse under extreme conditions. *Phil. Trans. R. Soc. A* **374**, 20160188.

Skamarock, W.C., J. Klemp, J. Dudhia, D. O. Gill, D. Barker, W. Wang, J. G. Powers, 2008: *A Description of the Advanced Research WRF Version 3.* 3-27. NCAR/TN–475+STR. NCAR Technical Note. p. 113.

Thompson, G., P. R. Field, R. M. Rasmussen, W. D. Hall, 2008: Explicit forecasts of winter precipitation using an improved bulk microphysics scheme. Part II: Implementation of a new snow parameterization. *Mon. Wea. Rev.*, **136**, 5095–5115.

Tewari, M., F. Chen, W. Wang, J. Dudhia, M. A. LeMone, K. Mitchell, M. Ek, G. Gayno, J. Wegiel, and R. H. Cuenca, 2004: Implementation and verification of the unified NOAH land surface model in the WRF Model. 20th Conference on Weather Analysis and Forecasting and 16th Conference on Numerical Weather Prediction, Seattle, pp. 11-15.

Turner, D. D., V. Wulfmeyer, A. Behrendt, T. A. Bonin, A. Choukulkar, R. K. Newsom, W. A. Brewer, and D. R. Cook, 2018: Response of the land-atmosphere system over north-central Oklahoma during the 2017 eclipse. *Geophysical Research Letters*, **45,** 1668–1675. https://doi.org/10.1002/2017GL076908

Wingo, S.M., and K. R. Knupp, 2015: Multi-platform observations characterizing the afternoon-to-evening transition of the planetary boundary layer in Northern Alabama, USA. *Boundary-Layer Meteor.*, **5,** 29-53.

Accepted for publication in *Bulletin of the American Meteorological Society.* DOI 10.1175/BAMS-D-19-0051.1.

Table 1. Modeled parameters without (with) solar forcing at 1705, 1825, and 1945 and the 1705-1945 UTC mean. Without solar forcing assumes solar eclipse. Totality occurred near 1825 UTC.

Location (by County)	Time (UTC)	*LE* (Wm^{-2})	*H* (Wm^{-2})	*RH* (%)	T_{air} (°C)	*WSPD* ($m\ s^{-1}$)	*WDIR* (°)	*PBLH* (m)
Warren	1705	357 (375)	161 (178)	51 (51)	31.8 (31.9)	2.9 (2.9)	191 (191)	1336 (1336)
	1825	7 (384)	-12 (176)	57 (47)	29.0 (32.5)	2.2 (2.1)	179 (190)	43 (930)
	1945	317 (358)	117 (146)	50 (48)	31.7 (32.7)	3.8 (3.6)	177 (182)	1337 (1120)
	Mean	174 (380)	44 (172)	55 (48)	30.6 (32.5)	2.7 (2.8)	185 (190)	502 (1252)
Christian	1705	413 (447)	111 (133)	51 (51)	31.1 (31.2)	3.0 (3.0)	207 (207)	766 (766)
	1825	0 (471)	-15 (118)	53 (44)	28.0 (32.1)	1.7 (1.9)	233 (236)	43 (1591)
	1945	380 (434)	86 (91)	50 (44)	30.9 (32.4)	2.9 (2.6)	199 (196)	766 (1337)
	Mean	199 (461)	24 (116)	54 (46)	29.8 (32.0)	2.2 (2.5)	220 (222)	439 (1306)
Todd	1705	377(404)	137 (157)	52 (50)	31.7 (31.8)	2.7 (2.7)	207 (207)	1335 (1335)
	1825	3 (418)	-11 (155)	55 (47)	29.0 (32.5)	1.4 (2.0)	205 (214)	43 (1899)
	1945	341 (386)	107 (126)	50 (48)	31.5 (32.9)	3.0 (2.9)	197 (176)	1336 (1904)
	Mean	183 (409)	36 (151)	54 (48)	30.5 (32.4)	2.1 (2.2)	198 (204)	820 (1791)
Lewis	1705	424 (424)	179 (179)	54 (54)	31.0 (31.0)	3.7 (3.7)	237 (237)	1111 (1111)
	1825	44 (431)	-17 (168)	64 (50)	28.4 (31.7)	2.4 (3.8)	236 (236)	43 (1591)
	1945	334 (93)	104 (-19)	56 (58)	30.7 (29.9)	3.1 (2.5)	200 (211)	765 (1896)
	Mean	214 (400)	44 (151)	60 (52)	29.7 (31.5)	2.8 (3.5)	225 (231)	667 (1452)

Note: *LE* = Latent heat flux; *H* = Sensible heat flux; *RH* = Relative Humidity; T_{air} = Air Temperature; *WS* = Wind Speed; *WDIR* = Wind Direction; and *PBLH* = Planetary Boundary Layer Height.

Accepted for publication in *Bulletin of the American Meteorological Society.* DOI 10.1175/BAMS-D-19-0051.1.

Figure 1. The total solar eclipse of August 21, 2017. This photo was taken at Hopkinsville, KY. The location is shown as a diamond immediately east of the MoDLS in figure 2. (Photo: Courtesy of Joseph Matus)

Accepted for publication in *Bulletin of the American Meteorological Society.* DOI 10.1175/BAMS-D-19-0051.1.

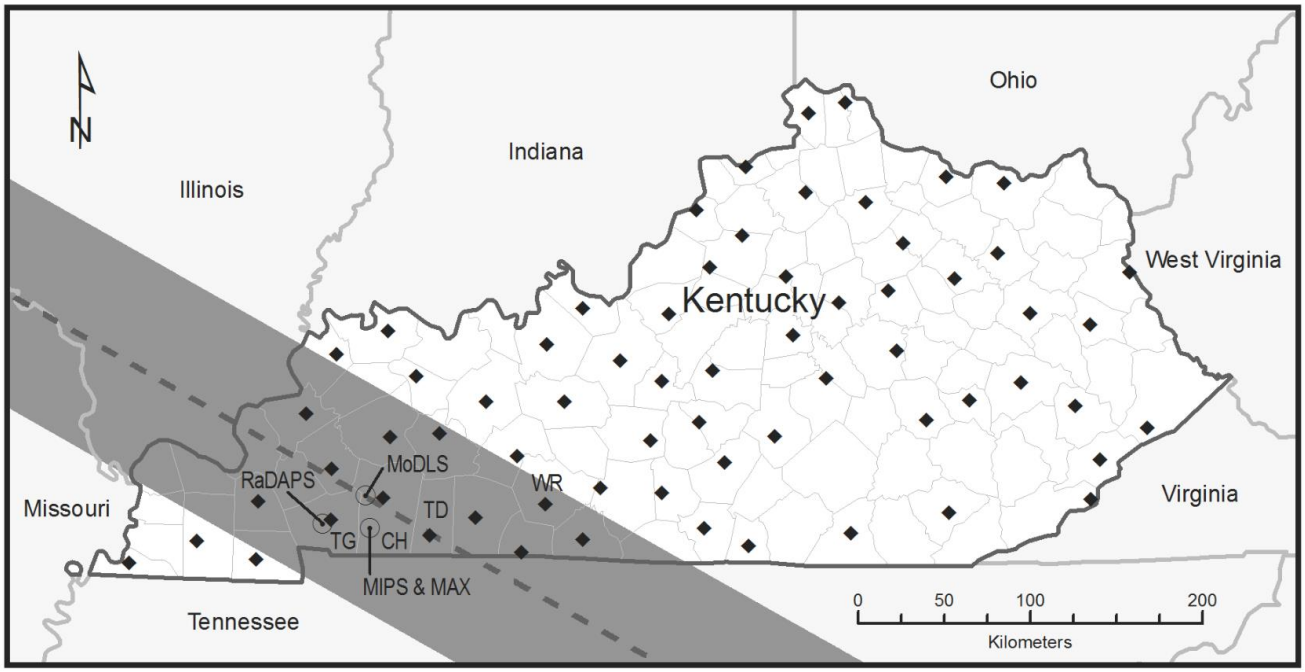

Figure 2. The Kentucky Mesonet, atmospheric profiling systems, the path of the solar eclipse, and the named counties. In the map, MoDLS = Mobile Doppler Lidar and Sounding System; MIPS = Mobile Integrated Profiling System (MIPS), RaDAPS= Rapidly Deployable Atmospheric Profiling System; and Mobile Alabama X-band radar (MAX). Named counties: WR-Warren, TD-Todd, CH-Christian, and TG-Trigg.

Accepted for publication in *Bulletin of the American Meteorological Society.* DOI 10.1175/BAMS-D-19-0051.1.

a)

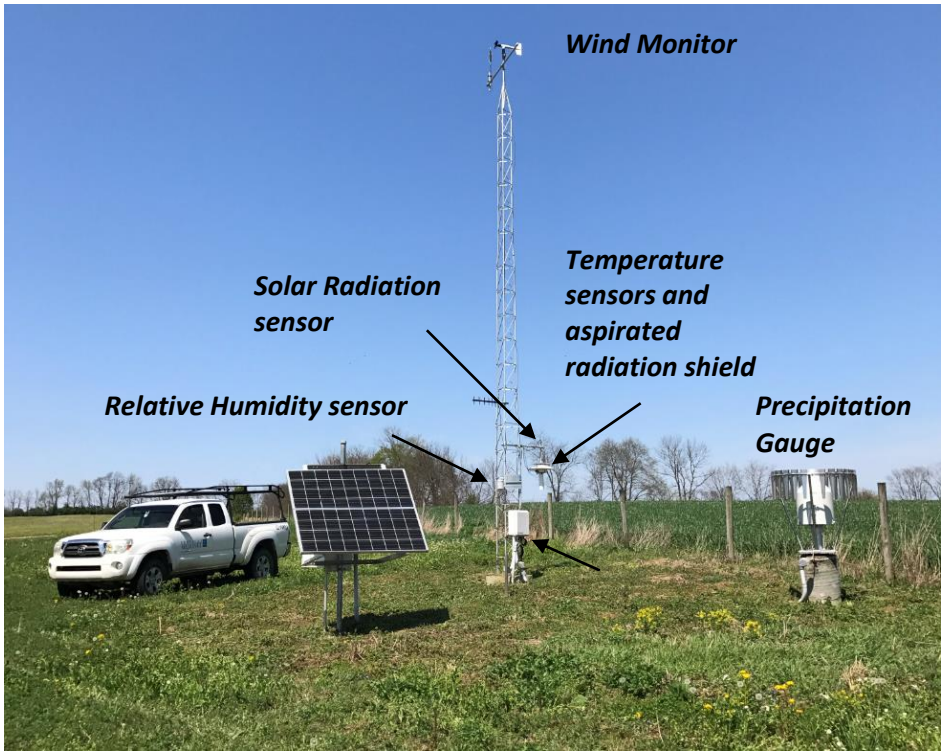

b)

Accepted for publication in *Bulletin of the American Meteorological Society.* DOI 10.1175/BAMS-D-19-0051.1.

c)

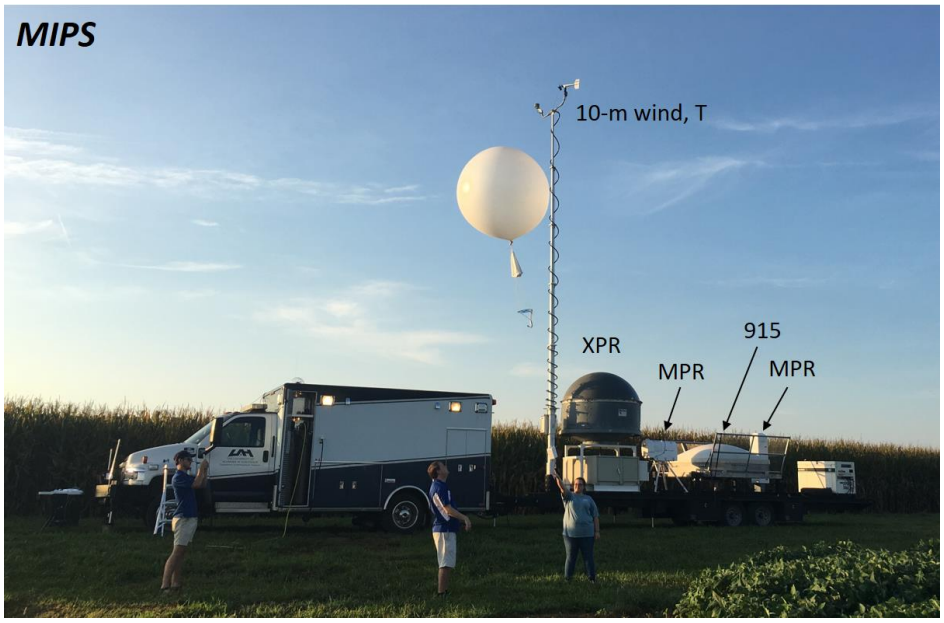

d)

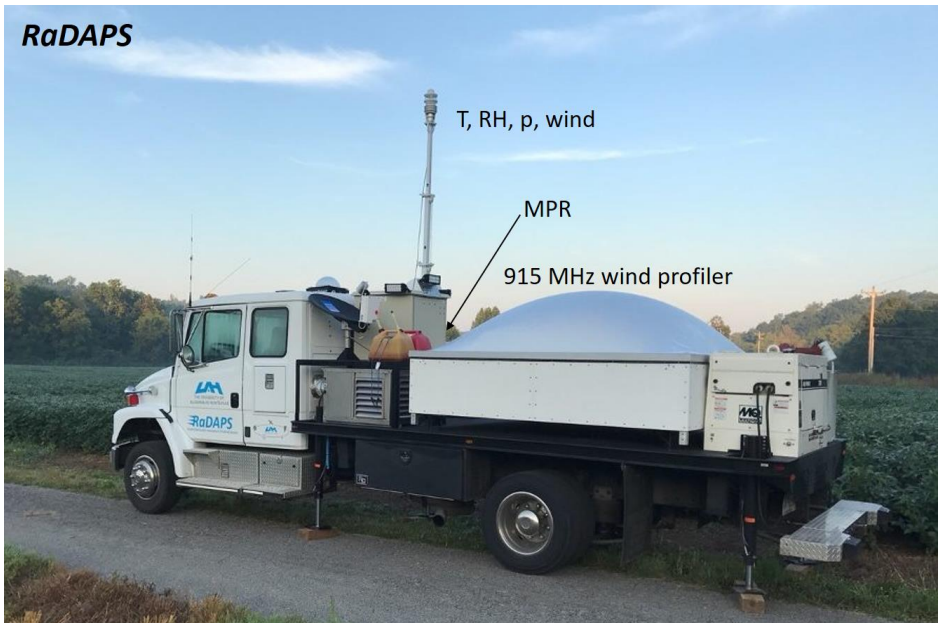

Accepted for publication in *Bulletin of the American Meteorological Society.* DOI 10.1175/BAMS-D-19-0051.1.

e)

Figure 3a-e. a) A Kentucky Mesonet station, b) Mobile Doppler Lidar and Sounding System (MoDLS), c) Mobile Integrated Profiling System (MIPS), d) Rapidly Deployable Atmospheric Profiling System (RADAPS), and Mobile Alabama X-band (MAX) radar.

Accepted for publication in *Bulletin of the American Meteorological Society.* DOI 10.1175/BAMS-D-19-0051.1.

a)

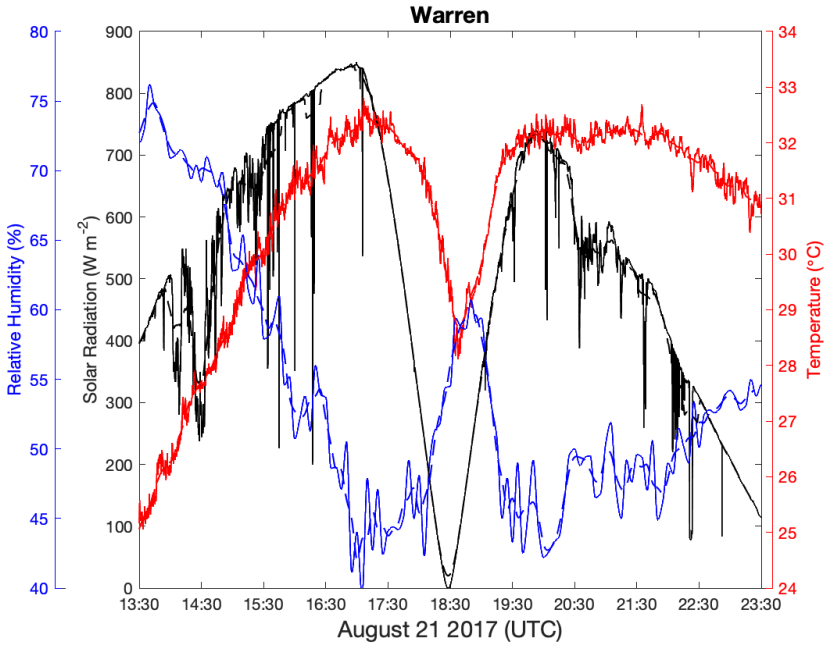

b)

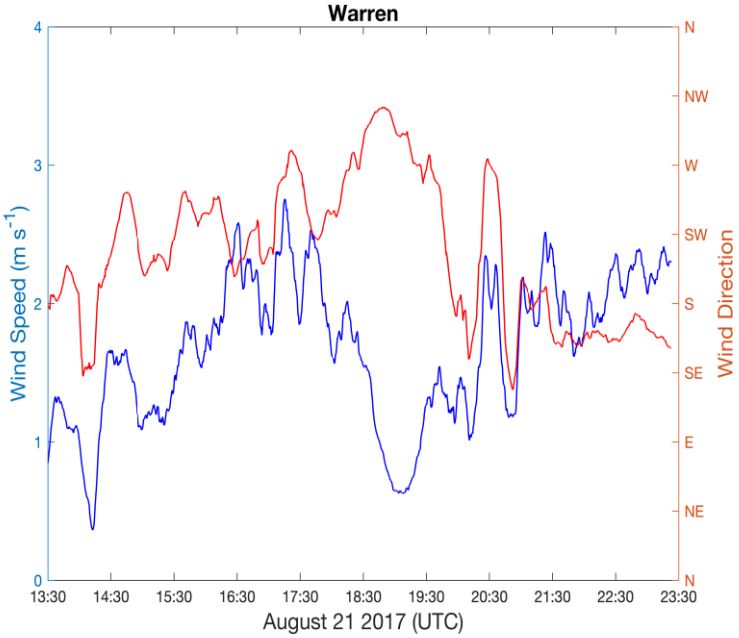

Figure 4. a) Solar radiation (W m^{-2}), air temperature (°C), and relative humidity (%) measured by the Kentucky Mesonet at three second intervals in Warren County, KY. Dashed lines present the raw data and the solid lines show the data smoothed using a five minute moving average. All additional plots will show just the smoothed data. b) Wind speed and direction.

Accepted for publication in *Bulletin of the American Meteorological Society.* DOI 10.1175/BAMS-D-19-0051.1.

a)

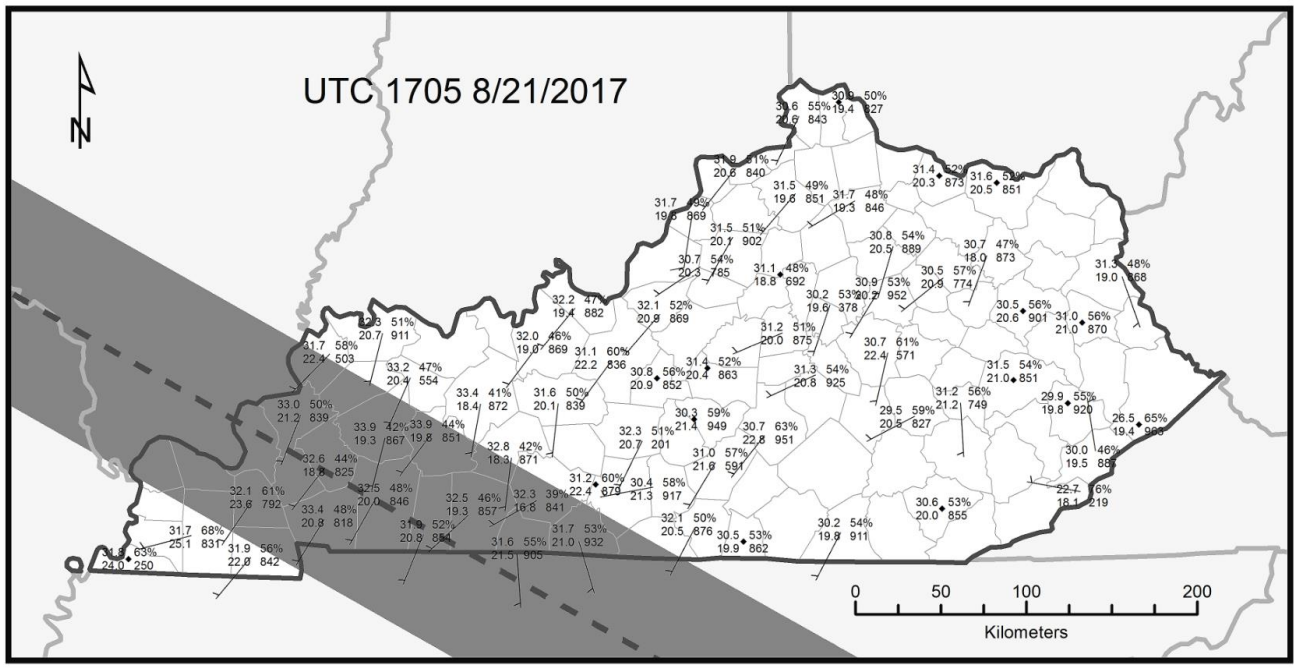

b)

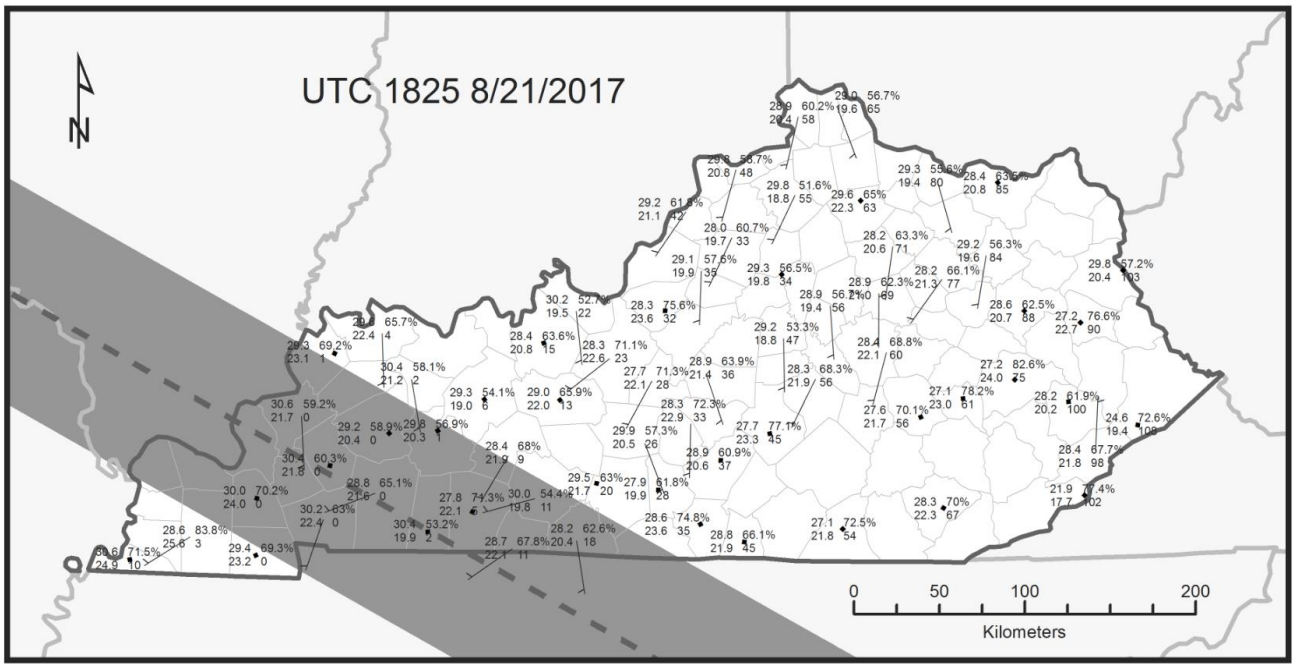

Accepted for publication in *Bulletin of the American Meteorological Society.* DOI 10.1175/BAMS-D-19-0051.1.

c)

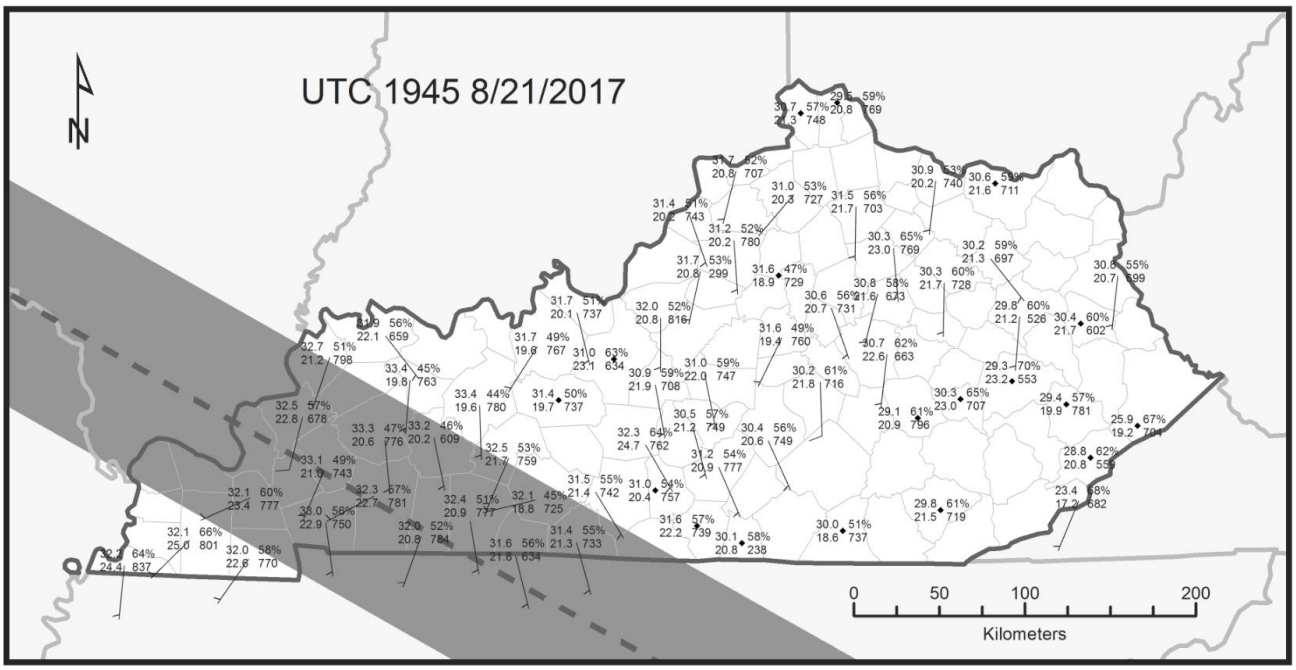

Figure 5a-c. Response of meteorological variables: a) at the beginning of the solar eclipse, b) near total solar eclipse, and c) near the end of the eclipse. For all stations, larger values on the left side represent temperatures and lower values on the left side represent dew point temperature (both in °C), values with percent unit are relative humidity and values on the lower right are solar radiation (W m^{-2}), and wind barbs are showing the direction from which the wind is blowing.

Accepted for publication in *Bulletin of the American Meteorological Society.* DOI 10.1175/BAMS-D-19-0051.1.

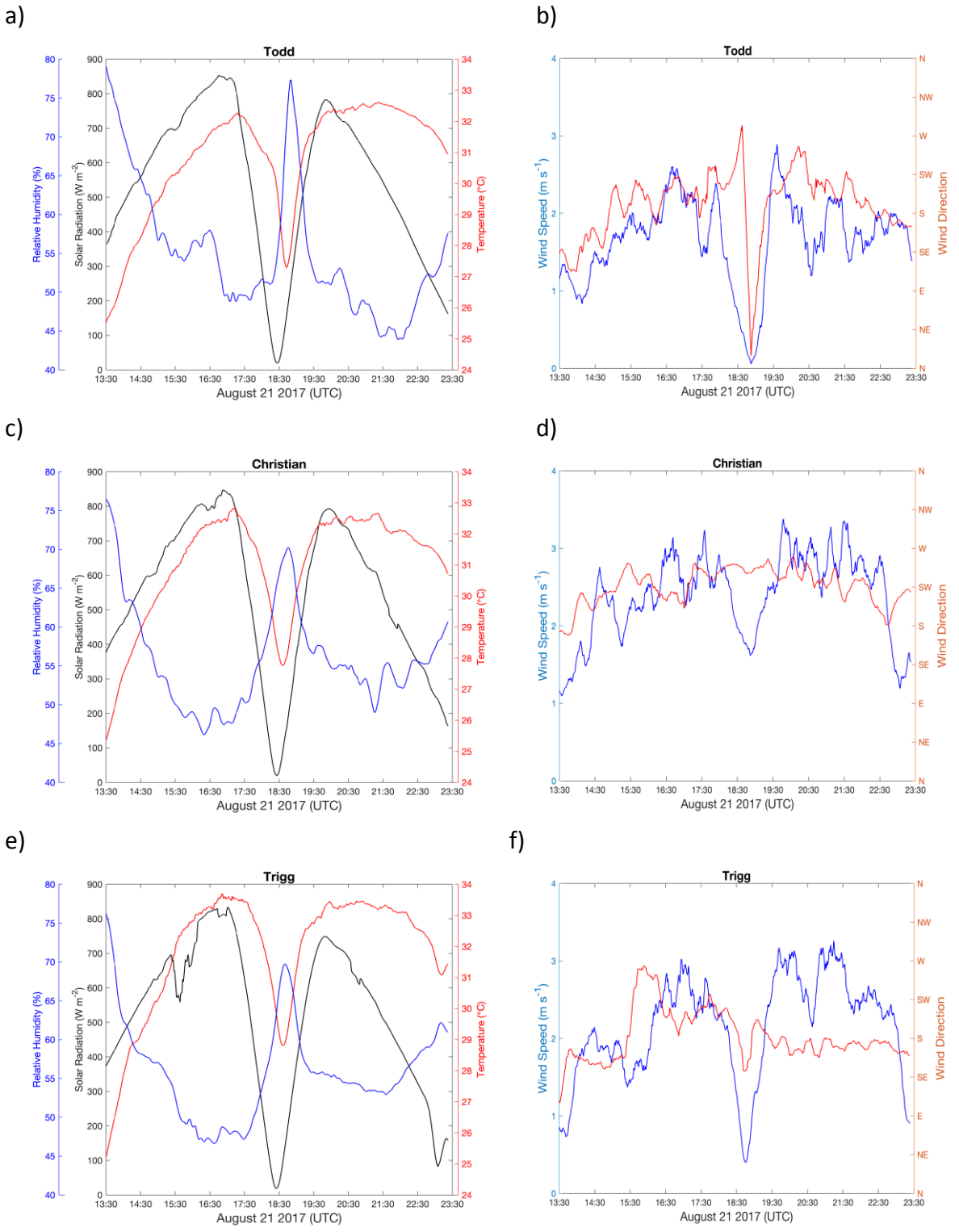

Figure 6a-f. a, c, and e) solar radiation, air temperature, and relative humidity and b, d, and f) wind speed and direction for Todd, Christian, and Trigg county mesonet stations during partial and total solar eclipse.

Accepted for publication in *Bulletin of the American Meteorological Society.* DOI 10.1175/BAMS-D-19-0051.1.

a)

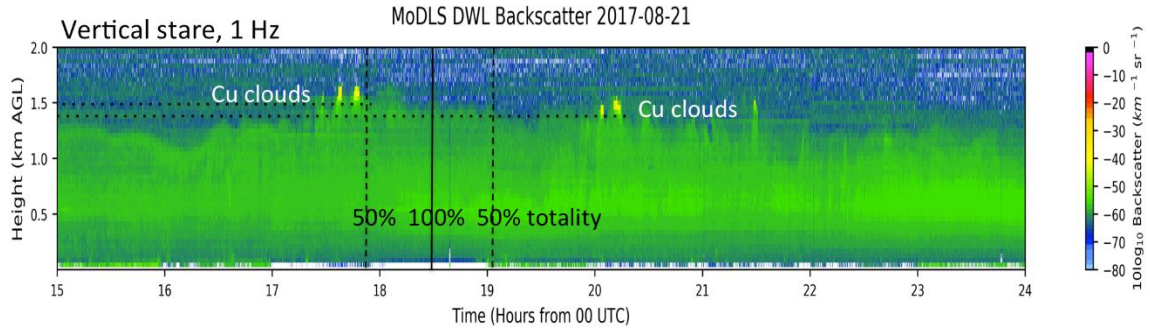

b)

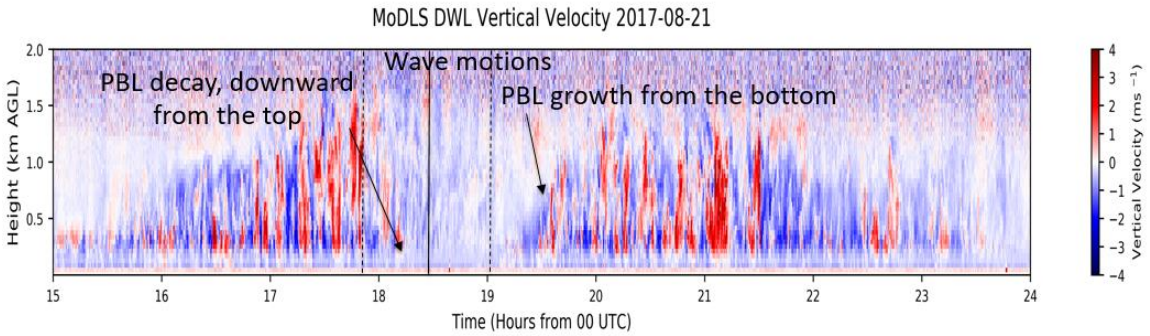

Figure 7a-b. Time vs. height section of Doppler wind lidar backscatter and vertical motion from the MoDLS site between 1500 and 0000 UTC.

Accepted for publication in *Bulletin of the American Meteorological Society.* DOI 10.1175/BAMS-D-19-0051.1.

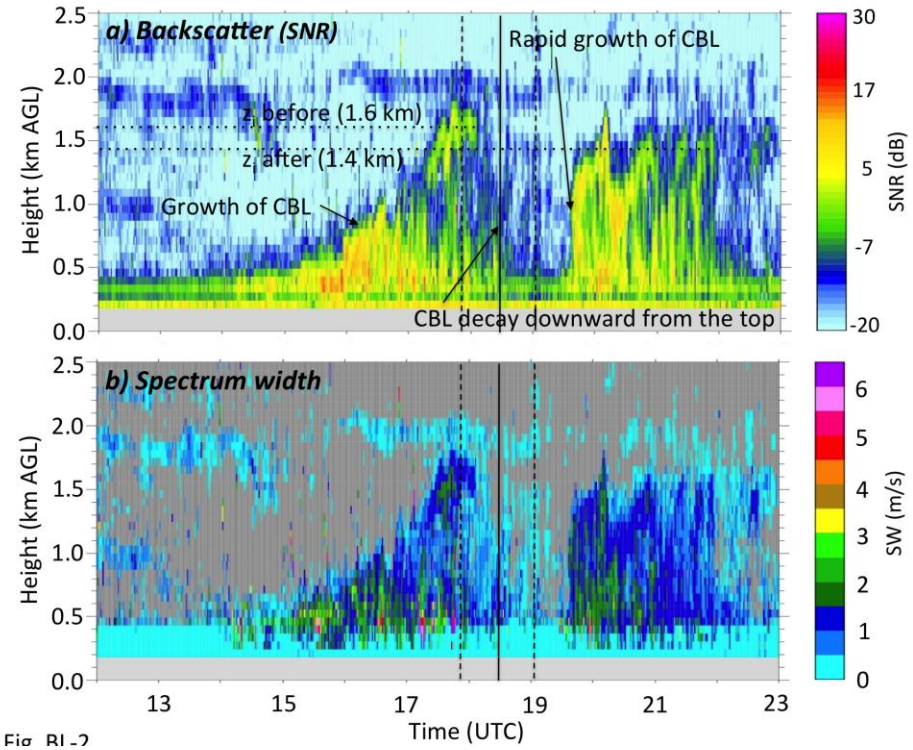

Figure 8a-b. Time vs. height section of SNR and spectrum width from the MIPS 915 MHz Doppler wind profiler site between 1200 and 2300 UTC.

Accepted for publication in *Bulletin of the American Meteorological Society.* DOI 10.1175/BAMS-D-19-0051.1.

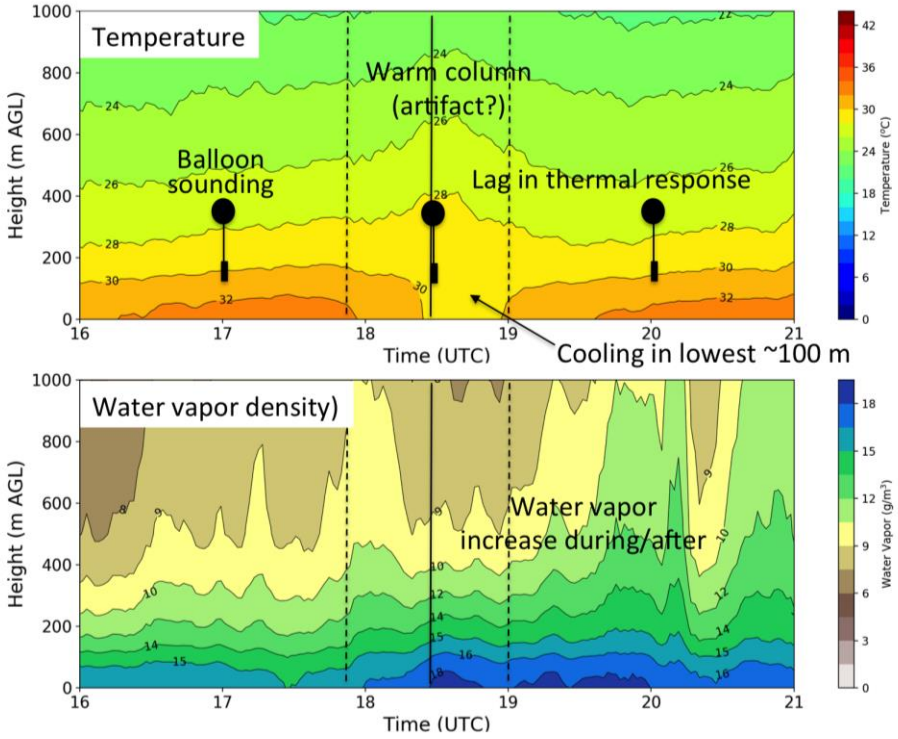

Figure 9a-b. Time vs. height sections of retrieved temperature and water vapor density from a microwave profiling radiometer located at the MIPS site. Time of balloon soundings are shown for 1700, 1830, and 2000 UTC. Temperature and water vapor density is contoured at 2 °C and 1.5 kg m^{-3} intervals, respectively.

Accepted for publication in *Bulletin of the American Meteorological Society.* DOI 10.1175/BAMS-D-19-0051.1.

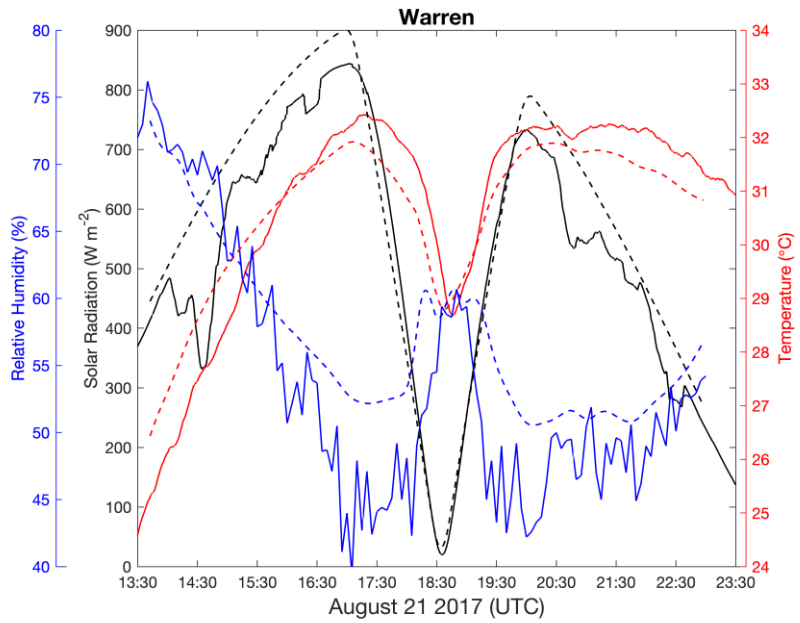

Figure 10. Solar radiation (Wm^{-2}), air temperature (°C), relative humidity (%) measured by the Kentucky Mesonet in Bowling Green, KY (solid) and a WRF simulation of the eclipse (dashed).

Accepted for publication in *Bulletin of the American Meteorological Society.* DOI 10.1175/BAMS-D-19-0051.1.

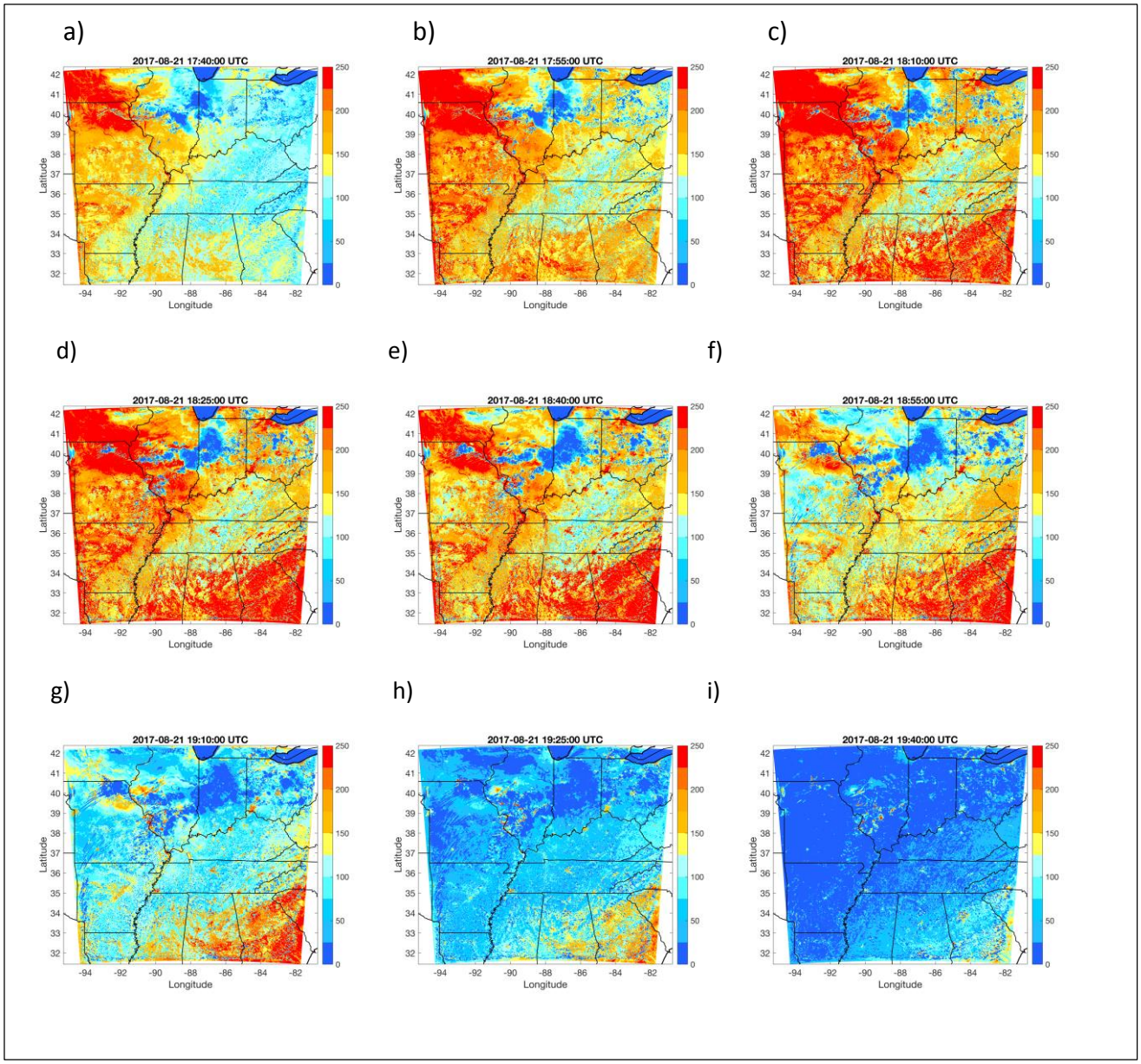

Figure 11a-i. Sensible heat flux (W m^{-2}, instantaneous) difference: without minus with solar eclipse.

Accepted for publication in *Bulletin of the American Meteorological Society.* DOI 10.1175/BAMS-D-19-0051.1.

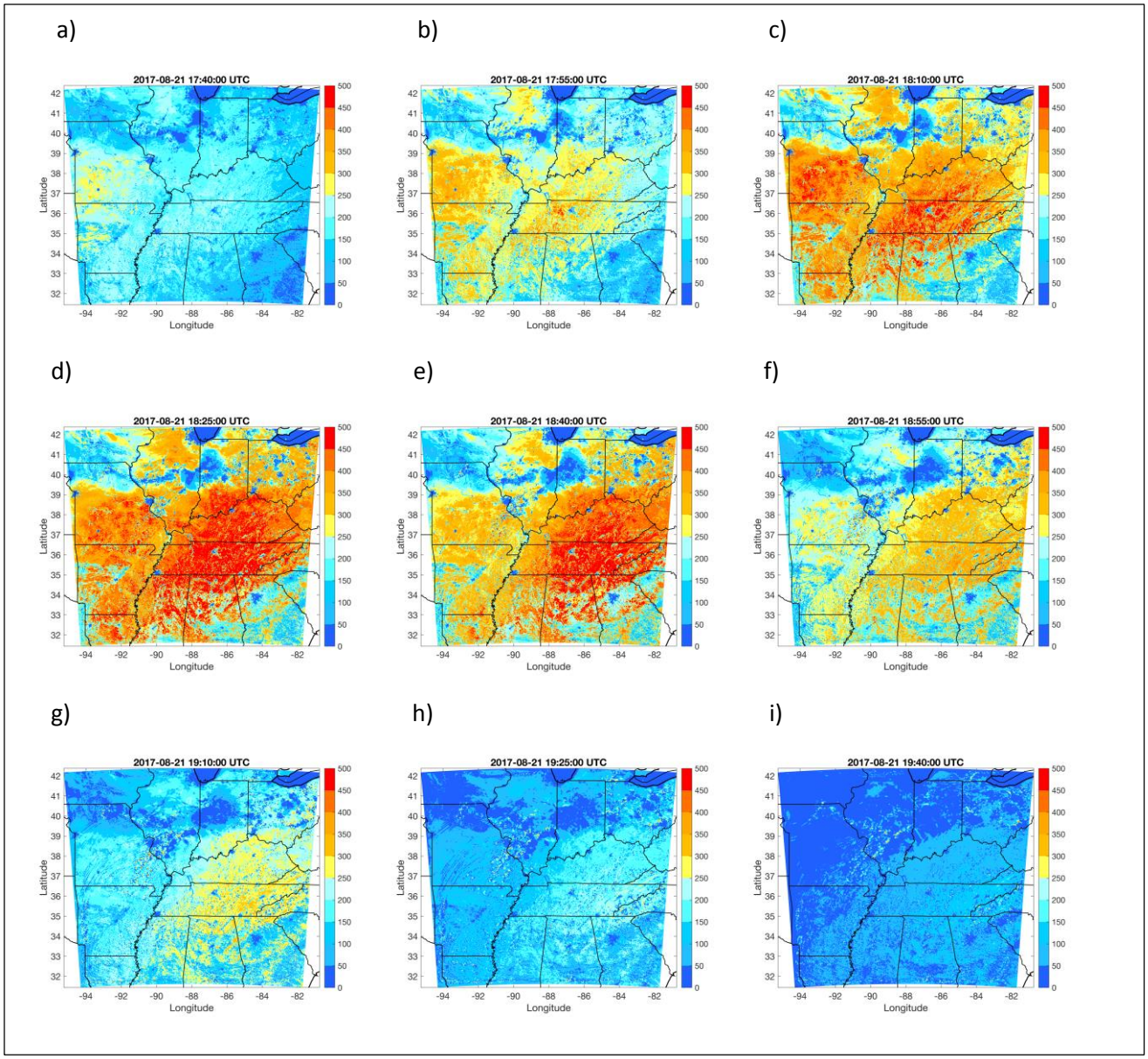

Figure 12a-i. Latent heat flux (W m^{-2}, instantaneous) difference: without minus with solar eclipse.

Accepted for publication in *Bulletin of the American Meteorological Society.* DOI 10.1175/BAMS-D-19-0051.1.